

Unveiling alkali metal poisoning of Cr—Mn catalyst for selective catalytic reduction of NO_x with NH₃: An experimental and theoretical study



Ninghan Wei^b, Xiaomei Hu^a, Cheng Zhao^a, Zhangfa Tong^b, Junge Yun^c, Xueying Jiang^b, Keju Wang^b, Yun Zou^{b,*}, Zhihang Chen^{a,c,**}

^a Guangdong Key Lab of Water & Air Pollution Control, Guangdong Province Engineering Laboratory for Air Pollution Control, South China Institute of Environmental Sciences, Ministry of Ecology and Environment, Guangzhou 510655, PR China

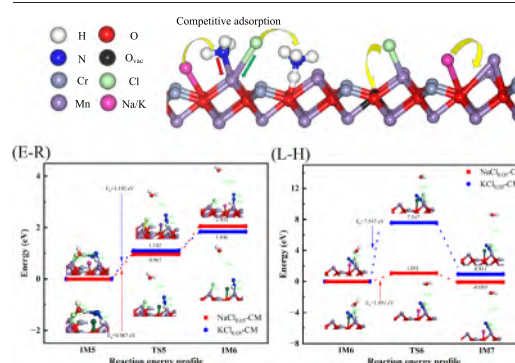
^b Guangxi Key Laboratory of Petrochemical Resource Processing and Process Intensification Technology, School of Chemistry and Chemical Engineering, Guangxi University, Nanning 530004, PR China

^c College of Environment and Resources, Xiangtan University, Xiangtan 411105, PR China

HIGHLIGHTS

- NaCl/KCl can seriously poison the physicochemical properties of CM catalyst.
- NaCl cut off E-R mechanism reactions.
- Cl adsorption is major cause diminishing Lewis/Brønsted acid and oxygen vacancies.
- Na/K can weaken Mn—O bond and impede NO adsorption/activation.
- NaCl/KCl increases the reaction heat and energy barrier of rate-controlling step.

GRAPHICAL ABSTRACT



ARTICLE INFO

Editor: Daniel CW Tsang

Keywords:

Alkali metal poisoning
NH₃-SCR
Cr-Mn
DFT calculations

ABSTRACT

Alkali metal poisoning has been an intricate and unsolved issue confining the catalytic activity of NH₃-SCR catalysts up to now. Herein, the effect of NaCl and KCl on catalytic activity of Cr—Mn catalyst for NH₃-SCR of NO_x was systematically investigated to clarify the alkali metal poisoning by combined experiments and theoretical calculations. It unveiled that NaCl/KCl could deactivate Cr—Mn catalyst due to the decrease in specific surface area, electron transfer ($\text{Cr}^{5+} + \text{Mn}^{3+} \leftrightarrow \text{Cr}^{3+} + \text{Mn}^{4+}$), redox ability and oxygen vacancy and NH₃/NO adsorption. In addition, NaCl cut off E-R mechanism reactions by inactivating surface Brønsted/Lewis acid sites. DFT calculations revealed that (1) Na and K could weaken Mn—O bond, (2) competitive adsorption between Cl and NH₃ was a main reason weakening Lewis acid, (3) Cl adsorption was also a major cause diminishing Brønsted acid and oxygen vacancy, (4) Both Na and K seriously impeded NO adsorption/activation, (5) NaCl/KCl increased the reaction heat of H₂O desorption (rate-determining step) in E-R mechanism reactions and KCl elevated its energy barrier in L-H mechanism reactions. Thus, this study provides the deep understanding of alkali metal poisoning and a well strategy to synthesize NH₃-SCR catalysts with outstanding alkali metal resistance.

* Corresponding author.

** Correspondence to: Z. Chen, Guangdong Key Lab of Water & Air Pollution Control, Guangdong Province Engineering Laboratory for Air Pollution Control, South China Institute of Environmental Sciences, Ministry of Ecology and Environment, Guangzhou 510655, PR China.

E-mail addresses: zouyun@gxu.edu.cn (Y. Zou), chenzhihang@scies.org (Z. Chen).

<http://dx.doi.org/10.1016/j.scitotenv.2023.162294>

Received 3 November 2022; Received in revised form 9 February 2023; Accepted 13 February 2023

Available online 16 February 2023

0048-9697/© 2023 Published by Elsevier B.V.

1. Introduction

Nitrogen oxides (NO_x), originated from mobile and stationary sources, are regarded as the major causes leading to global warming, ozone layer depletion, photochemical smog, acid rain and fine particles, thereby influencing the life and health of plants and animals (Lian et al., 2022). With the growing desire for good air quality, the emission reduction of NO_x have been concerned many countries and areas. Chinese government issues the standard (GB 13223-2011) to limit NO_x emission concentration below 100 mg/m³ for the new coal-fired power plants and below 50 mg/m³ for the gas turbine power plants. In addition, strict emission limits for non-electric industries, such as cement, glass and ceramic, are also required. Therefore, it is urgent to address NO_x emission properly. Among numerous treatment methods (H₂-SCR, SNCR and NH₃-SCR), selective catalytic reduction (NH₃-SCR) of NO using NH₃ as one of the most effective technologies to abate NO_x has been universally used in exhaust aftertreatment system (Liu et al., 2021a). Though commercial V₂O₅-WO₃/TiO₂ has been widely used to eliminate NO_x to date, its further utilization in industrial production was greatly obstructed by some disadvantages, such as narrow temperature window (300–400 °C), toxicity of vanadium and easy deactivation (Hou et al., 2021). In addition, the SCR equipment is installed in the downstream of dedusting and desulfurization units, so the flue gas temperature further decreases below 300 °C. Therefore, many researchers are dedicated to investigating low-temperature and eco-friendly SCR catalysts.

Recently, Mn-based catalysts have attracted considerable interests due to their excellent catalytic performance at low-temperature, low cost, abundance in the earth and environmentally friendly character (Choi et al., 2016; Yao et al., 2019). Among them, Cr—Mn catalysts and their ramifications, such as CrMn_{1.5}O₄ (Chen et al., 2009), MnCr₂O₄ (Gao et al., 2020b), CrMn₂O₄ (Gao et al., 2019), Ce-Mn-Cr layered double oxide (Yoon et al., 2022) and Mn_xCo_{1-x}Cr₂O₄ spinel-type catalyst (Gao et al., 2020a), exhibits outstanding low-temperature activity and wide temperature window, so they have been regarded as potential candidates for V-based catalysts during NH₃-SCR reactions. However, some challenges still remain when Cr—Mn catalysts and their derivatives are utilized in the post-treatment system of exhaust gases. Therein, alkali metals adsorbed on surface active sites of the catalysts could bring about a dramatic decline in catalytic performance. Hence, it is desired to investigate their poisoning mechanism by alkali metals.

In the practical industrial production, NaCl and KCl (alkali metals) in the flue gas, emitted from stationary sources (coal-fired and biomass-fired power plants), are inevitably involved in NH₃-SCR reactions to shorten the lifetime of SCR catalysts (Jiang et al., 2020a; Jiang et al., 2020b). According to previous experimental researches, the poisoning reasons of SCR catalysts by Na and K were concluded as followed: (1) suppressing NH₃ adsorption/activation by interacting with active sites or competitive adsorption, (2) forming inactive NO_x species and (3) blocking pore channels and decreasing specific surface area and redox capacity (Fang et al., 2019a; Li et al., 2020; Wang et al., 2017). Furthermore, the effect of Na and K on the surface properties of SCR catalysts at atomic level was revealed by theoretical calculations. It has been reported that Na and K could adsorb on CeO₂-WO₃ catalyst (110) surface and promote surface oxygen cover active W site, thereby inhibiting NH₃ adsorption (Peng et al., 2012a). Some researchers revealed that K not only increased the adsorption energy for NH₃ on Lewis acid sites and for NH₄⁺ on Brønsted acid sites, but also inhibited the formation of chemisorbed oxygens and oxygen vacancies (Jiang et al., 2021b). The effect of K on the SCR performance of V₂O₅/TiO₂ was also investigated, and it was found that K atom decreased surface acidity by accelerating electrons transfer from K to O atom, and K also led wider band gap of V₂O₅/TiO₂ from 0.74 to 0.81 eV, thereby decreasing its reducibility (Peng et al., 2012b).

To the best of our knowledge, most of theoretical researches focus on V-based and Ce-based catalysts, but few on promising Mn-based catalysts. The poisoning effect of Na and K, the poisoning effect of single Cl anion and the synergistic effect of Na/K and Cl on SCR catalysts are hardly revealed. Furthermore, the effect of NaCl and KCl on the rate-controlling step of L-H/E-R mechanism reactions is unclear. In this work, promising CrMn_{1.5}O₄ catalyst

was impregnated by various NaCl or KCl contents and used for NH₃-SCR of NO_x. Then the poisoning effect of NaCl and KCl on textural properties, crystal structure, surface atomic distribution, redox ability, surface acidity and reaction mechanism of Cr—Mn catalyst was investigated by comprehensive characterizations. Moreover, DFT calculations were carried out to reveal N₂ formation pathways and the poisoning effect of Na, K, Cl, NaCl and KCl on surface species at atomic level. Eventually, based on reaction pathways, we further illustrated the effect of NaCl and KCl on the rate-controlling reaction steps. This study provides a comprehensive insight into alkali metal poisoning during NH₃-SCR reactions and a well strategy to synthesize SCR catalysts with outstanding alkali metal resistance.

2. Experimental method

2.1. Catalyst preparation

CrMn_{1.5}O₄ catalyst (denoted as CM) with 2:3 M ratio of (Cr(NO₃)₃·9H₂O)/(CH₃COO)₂·Mn·4H₂O) was prepared by coprecipitation method. Typically, (Cr(NO₃)₃·9H₂O (Aldrich Co., 99.0 wt%) and (CH₃COO)₂·Mn·4H₂O (Aldrich Co., 99.0 wt%) at room temperature were dissolved in the deionized water, and then 2.5 mol/L NH₃·H₂O with same volume as metal salt solution was added dropwise to the above solution. After stirring for 1 h and standing for 24 h, the precipitates were washed, filtered and dried at 120 °C for 12 h. The obtained samples were calcined at 650 °C for 3 h at the rate of 5 °C/min.

The NaCl-poisoned and KCl-poisoned catalysts were obtained by impregnation method. In detail, CM catalyst was fully immersed in 50 mL NaCl or KCl aqueous solutions (0.008 or 0.04 mol/L). Then water was evaporated to acquire NaCl and KCl containing samples. Finally, the samples were further calcined at 650 °C for 3 h under an air environment. The obtained catalysts were denoted as Na(K)Cl_x-CM, where x stood for the molar ratio of Na(K)/(Na(K) + Cr).

2.2. NH₃-SCR activity

1.44 mL catalysts (40–60 mesh, about 1.8 g) were fixed in a fixed-bed quartz reactor (inner diameter 8 mm) to determine NH₃-SCR activity within 80–300 °C. The feed mixed gases composed of 1000 ppm NH₃, 1000 ppm NO, 3% O₂ and N₂ balance gas. The total gas flow maintained at 1200 L/min, corresponding to a gas hourly space velocity (GHSV) of 50,000 h⁻¹. The reaction gas concentration was monitored by Testo 350 (Germany) and TELEDYNE T320 (America). The data was obtained strictly when the reaction remained stable state (above 25 min) at the chosen temperature. Related NO conversion and N₂ selectivity were defined as followed:

$$\text{NO conversion (\%)} = \frac{[\text{NO}]_{\text{in}} - [\text{NO}]_{\text{out}}}{[\text{NO}]_{\text{in}}} \times 100\%$$

$$\text{N}_2 \text{ selectivity (\%)} = \frac{[\text{NO}]_{\text{in}} + [\text{NH}_3]_{\text{in}} - [\text{NO}]_{\text{out}} - [\text{NH}_3]_{\text{out}} - [\text{NO}_2]_{\text{out}} - 2[\text{N}_2\text{O}]_{\text{out}}}{[\text{NO}]_{\text{in}} + [\text{NH}_3]_{\text{in}} - [\text{NO}]_{\text{out}} - [\text{NH}_3]_{\text{out}}} \times 100\%$$

2.3. Characterizations

XRD patterns were acquired by the 6100 X-ray diffraction analyzer using Cu Kα as radiation resource (λ = 0.1541 nm) with scanning range between 5 and 90° at a step rate of 6°/min. N₂ adsorption-desorption isotherm and pore structure data were obtained at 79 K with Micromeritics ASAP-2020. XPS spectra were recorded on a thermo Fisher Scientific K-Alpha electron spectroscopy.

NH₃-TPD experiments were operated on a multifunction chemisorption analyzer (TP-5080) with TCD. After He pretreatment at 350 °C for 1 h and cooled down to indoor temperature, the samples (0.1 g) were exposed in a

NH₃/He gas flow at 50 °C for 0.5 h. Subsequently, the samples were purged by He gases for 20 min. Finally, the samples were heated up to 800 °C at the rate of 10 °C/min in He flow. H₂-TPR experiments were also operated on a multifunction chemisorption analyzer (TP-5080) with TCD. The samples (0.1 g) were pretreated at 300 °C for 2 h in a steam of Ar and He. Then H₂/(Ar and He) mixture was fed into the reactor and the temperature increased from 100 to 800 °C at the rate of 10 °C/min. O₂-TPD experiments were conducted with a multifunction chemisorption analyzer (TP-5080) with TCD. Firstly, the samples (0.1 g) were pretreated O₂/He mixture at 280 °C for 1 h, and then cooled to 100 °C. Then the catalysts were exposed to O₂ for 30 min and followed by He. Finally, the temperature increased to 900 °C at the rate of 10 °C/min.

In situ DRIFTS experiments were recorded on a Bruker VERTEX 70 FTIR spectrometer and an MCT detector with a resolution of 4 cm⁻¹ and 64 scan numbers. The samples were pretreated in N₂ flow at 400 °C for 1 h before collecting background spectra. Related test conditions consisted of 100 mL/min total gas flow, 1000 ppm NH₃, 1000 ppm NO, 3% O₂ and N₂ balance.

2.4. DFT calculations

CASTEP package (Materials Studio 2017R2 from Accelrys) was used to operate all calculations (Lyu et al., 2020). Generalized gradient approximation (PBE) with Perdew-Burke-Ernzerhof (PBE) functional was employed to calculate the exchange-correlation potential (Liu et al., 2021c). The ultrasoft pseudopotential was used to figure out the mutual effect of the ionic core and the valence electrons. A plane-wave basis set with the spin polarization and cutoff energy of 340 eV was applied to expand the electronic wave functions. The (2 × 2 × 1) k-points were designed for the surface Brillouin zone integration. The convergence values during the geometry optimization and energy calculations consisted of self-consistent field energy (1 × 10⁻⁵ Ha), atomic displacement (5 × 10⁻³ Å) and energy gradient (2 × 10⁻³ Ha/Å).

The adsorption energy (E_{ads}) for gaseous molecular and oxygen vacancy formation energy (E_{ov}) was defined as followed:

$$E_{ads} = E_s - (E_{pf} + E_{sm})$$

$$E_{ov} = (E_{ovs} + E_o) - E_{pf}$$

where E_s, E_{pf}, E_{sm}, E_{ovs} and E_o were total energy of the system after adsorption, pure facet, small molecule, oxygen vacancy system and oxygen atom, respectively.

Herein, NH₃-SCR reaction steps involving N₂ and H₂O formation over CM catalyst were searched by the LST/QST method (Ren et al., 2021). NH₃-SCR reactions contained intermediates (IM) and transition states (TS). The reaction energy barrier (E_a) was defined as follow:

$$E_a = E_{TS} - E_{IM1}$$

$$E_{rh} = E_{IM2} - E_{IM1}$$

where E_{IM} and E_{TS} were the total energy of transition states and intermediates, respectively. The smaller E_a was, the more likely the reaction happened. The negative E_{rh} presented that this reaction was exothermic.

In the simulation, a (2 × 2) periodic CrMn_{1.5}O₄ (111) slab model was originated from CrMn_{1.5}O₄ conventional cell (Fig. S1a). As shown in Fig. S1b, (111) facet as common crystal facet presented threefold-coordinated Cr atom (Cr_{3c}), threefold-coordinated Mn atom (Mn_{3c}) and threefold-coordinated O atom (O_{3c}). The CrMn_{1.5}O₄ slab model consisted of total 10 atomic layers, corresponding to 92 atoms. The related oxygen vacancy models were obtained by deleting an oxygen connected Cr with Mn on (111) facet surface layer. During the calculation, the bottom half atoms were immobilized, while the top half atoms and small molecules were fully relaxed with the purpose of reducing the calculation time. A 18 Å vacuum slab was set to prevent the interaction between the adjacent surface (Pan et al., 2021a).

3. Results and discussion

3.1. NH₃-SCR activity

NO conversion of fresh, NaCl-poisoned and KCl-poisoned CM catalysts was simultaneously measured to shed light on the poisoning effect of NaCl and KCl on the catalytic activity of CM catalyst and related results were shown in Fig. 1. Note that the NO conversion of fresh CM catalyst was 100% NO conversion within 160–240 °C, and over 90% NO conversion was acquired in the range of 148–296 °C. However, NaCl and KCl addition exhibited an obvious inhibitory effect on NO conversion in the entire temperature range. Specifically, the order of activity loss was ranked by KCl_{0.05}-CM > NaCl_{0.05}-CM > KCl_{0.01}-CM > NaCl_{0.01}-CM, indicating that both NaCl and KCl seriously poisoned CM catalyst and KCl exhibited stronger toxicity than NaCl. As shown in Fig. S2, NaCl and KCl did not almost reduce N₂ selectivity of CM catalyst, which might be because of reduced redox reducibility inhibiting the further oxidation of -NH₂.

3.2. Crystal structure and textural properties

The effect of NaCl and KCl introduction on the crystal structure of CM catalyst was characterized by XRD (Fig. 2a). Pristine CM catalyst exhibited the characteristic diffraction peaks assigned to CrMn_{1.5}O₄ phase (PDF#71-0982). Relatively weak peaks ascribed to Cr₂O₃ phase (PDF#89-4836) and no extra diffractions ascribed to NaCl or KCl were observed (Chen et al., 2010). It indicated that NaCl and KCl were homogeneously dispersed on the CM catalyst surface or aggregated in tiny sizes that were beyond XRD detection limit (Liu et al., 2021b). However, the peak intensities of KCl_{0.05}-CM and NaCl_{0.05}-CM increased significantly, suggesting that there was strong interaction between NaCl/KCl and CM catalyst, and KCl and NaCl were beneficial for its crystallization (Li et al., 2019a).

N₂ adsorption-desorption experiments were conducted to further probe the effect of NaCl and KCl deposition on the textural properties of CM catalyst (Fig. 2b). All catalysts exhibited type IV isotherms with H3 type hysteresis loops, suggesting the appearance of mesoporous structure (Zheng et al., 2022). BET surface area, pore volume and pore size (Table 1) significantly reduced after NaCl and KCl introduction. It was because NaCl and KCl could block pore channel and cover the surface of CM catalyst, thereby suppressing the exposure of active sites (Li et al., 2020). Compare with NaCl_{0.05}-CM, KCl_{0.05}-CM with higher specific surface area exhibited lower NO conversion, indicating that specific surface area might not be the main reasons determining NH₃-SCR activity.

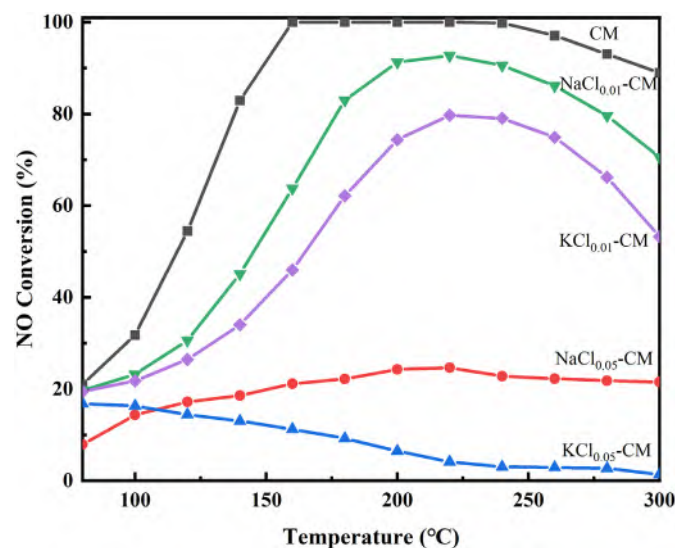


Fig. 1. NO conversion of CM, NaCl_{0.05}-CM and KCl_{0.05}-CM catalysts.

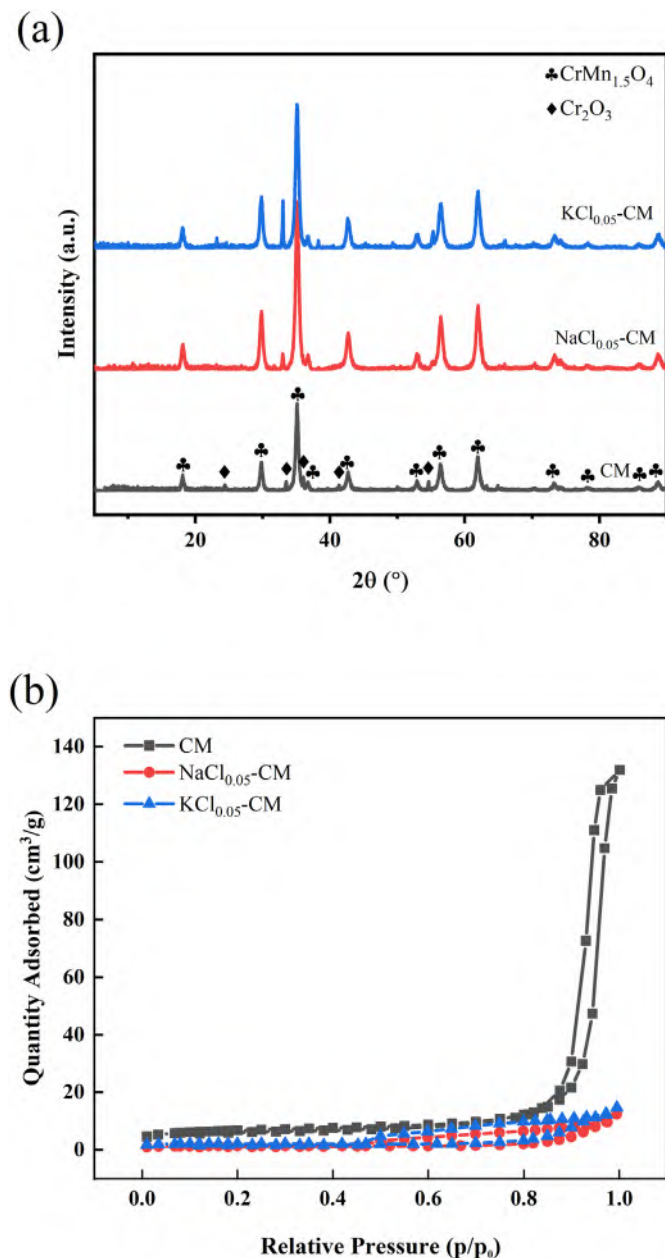


Fig. 2. XRD patterns (a) and N_2 adsorption-desorption isotherms (b) of CM, $NaCl_{0.05}$ -CM and $KCl_{0.05}$ -CM catalysts.

3.3. Surface chemical properties

The influence of NaCl and KCl deposition on the valence states distribution of the surface atoms over CM catalyst was investigated by XPS. The XPS spectra of Cr $2p_{3/2}$ (Fig. 3a) could be separated into three peaks, among

Table 1

BET results, valence state distributions of surface atoms and NH_3 desorption peak area.

Catalysts	BET surface area (m^2/g) ^a	Total pore volume (cm^3/g) ^a	Average pore size (nm) ^a	Cr ⁵⁺ /Cr ^b	Mn ⁴⁺ /Mn ^b	O _α /O ^b	All peak area ^c
CM	23.55	0.19	25.00	9.55%	26.09%	71.88%	0.39
$NaCl_{0.05}$ -CM	4.59	0.02	7.08	17.76%	19.06%	67.96%	0.14
$KCl_{0.05}$ -CM	7.24	0.02	5.68	19.33%	10.66%	62.61%	0.09

^a Obtained from BET.

^b Obtained from XPS.

^c obtained from NH_3 -TPD.

which peaks centered at 574.7–575.6, 575.4–576.7 and 577.4–578.4 eV were assigned to Cr²⁺, Cr³⁺ and Cr⁵⁺, respectively (Chen et al., 2010). The ratio of Cr⁵⁺/(Cr⁵⁺ + Cr³⁺ + Cr²⁺) could be calculated based on the peak area of Cr⁵⁺, Cr³⁺ and Cr²⁺. The Cr⁵⁺/Cr ratio for CM, $NaCl_{0.05}$ -CM and $KCl_{0.05}$ -CM was 9.55%, 17.76% and 19.33%, respectively. It was well-established that Cr⁵⁺ have a significant effect on NH_3 -SCR reactions, but Cr⁵⁺ concentration in this study exhibited the opposite trend as the NH_3 -SCR activity sequence because NaCl and KCl could suppress the redox cycle: Cr⁵⁺ + Mn³⁺ → Cr³⁺ + Mn⁴⁺ (Gao et al., 2020b; Gao et al., 2019). The decrease of electron transfer between Mn and Cr was a significant cause reducing SCR activity (Gao et al., 2019).

Mn⁴⁺ could oxidize NO into NO₂ due to well redox capacity, thereby promoting the “Fast-SCR” reaction ($2NO + 2NO_2 + 4NH_3 \rightarrow 4N_2 + 6H_2O$) (Li et al., 2021b). In addition, Mn⁴⁺ could bring about more oxygen vacancies (○): $2Mn^{4+} + O^{2-} \rightarrow 2Mn^{4+} + 2e^- + \text{○} + \frac{1}{2}O_2 \rightarrow \frac{1}{2}Mn^{4+} + Mn^{3+} + \frac{1}{2}Mn^{2+} + \text{○} + \frac{1}{2}O_2$, thereby accelerating NH_3 -SCR reactions (Xie et al., 2019). The XPS spectra of Mn $2p_{3/2}$ (Fig. 3b) could be split into three peaks at 639.9–640.6, 640.7–641.9 and 642.8–643.4 eV, which were ascribed to Mn²⁺, Mn³⁺ and Mn⁴⁺, respectively (Li et al., 2021a). The Mn⁴⁺/Mn ratio for CM, $NaCl_{0.05}$ -CM and $KCl_{0.05}$ -CM was 26.09%, 19.06% and 10.66%, respectively, indicating that KCl and NaCl deposition could result in the decline of redox properties and suppress the formation of oxygen vacancies, thereby deactivating CM catalyst. KCl caused more serious losses of redox properties than NaCl as well as oxygen vacancies.

Oxygen vacancies were beneficial for gaseous O₂ adsorption/activation on the catalyst surface, and formed chemisorbed oxygen played a significant role in “Fast SCR” reactions (Li et al., 2019b). As shown in Fig. 3c, after Cl introduction, the formation energy of oxygen vacancies increased from 3.208 to 15.140 eV, declaring that Cl could go against the formation of oxygen vacancies. However, after Na or K addition, the formation energy of oxygen vacancies exhibited a downward trend, indicating that the strong interaction between Na/K and Cl could weaken the suppressing effect of Cl on oxygen vacancy formation.

It is known to all that chemisorbed oxygen (O_α) can exhibit higher reactive activity than lattice oxygen (O_β) owing to its good mobility, and it is favorable for the translation of NO into NO₂, which is favor of “Fast-SCR” reactions (Liu et al., 2021d). Fig. 3d exhibited the O 1s XPS spectra, and they could be decomposed into three peaks ascribed to hydroxyl groups (530.7–531.3 eV), O_α (528.8–529.8 eV) and O_β (527.7–528.7 eV), respectively (Youn et al., 2021). A slight decrease of O_α/(O_α + O_β + O_γ) from 71.88% to 67.96% and 62.61% was observed after NaCl and KCl deposition on CM catalyst, which was related to oxygen vacancies and oxide defects during SCR reactions. Above results indicated that oxygen species mainly exists in the form of O_α over CM and poisoned CM catalysts, the strong interaction between NaCl/KCl and CM catalyst could suppress chemisorbed oxygen formation and KCl exhibited stronger inhibition effect on chemisorbed oxygen formation than NaCl.

O₂-TPD experiments were used to investigate the effect of NaCl and KCl on the activity of oxygen species. As shown in Fig. 3e, all O₂-TPD curves exhibited two desorption peak in the range of 787–859 and 444–500 °C, corresponding to bulk lattice oxygen and surface adsorbed oxygen ions/surface lattice oxygen, respectively (Shen et al., 2020). Compared with CM catalyst, surface adsorbed oxygen ions/surface lattice oxygen peak of $NaCl_{0.05}$ -CM and $KCl_{0.05}$ -CM catalyst shifted to higher temperature range,

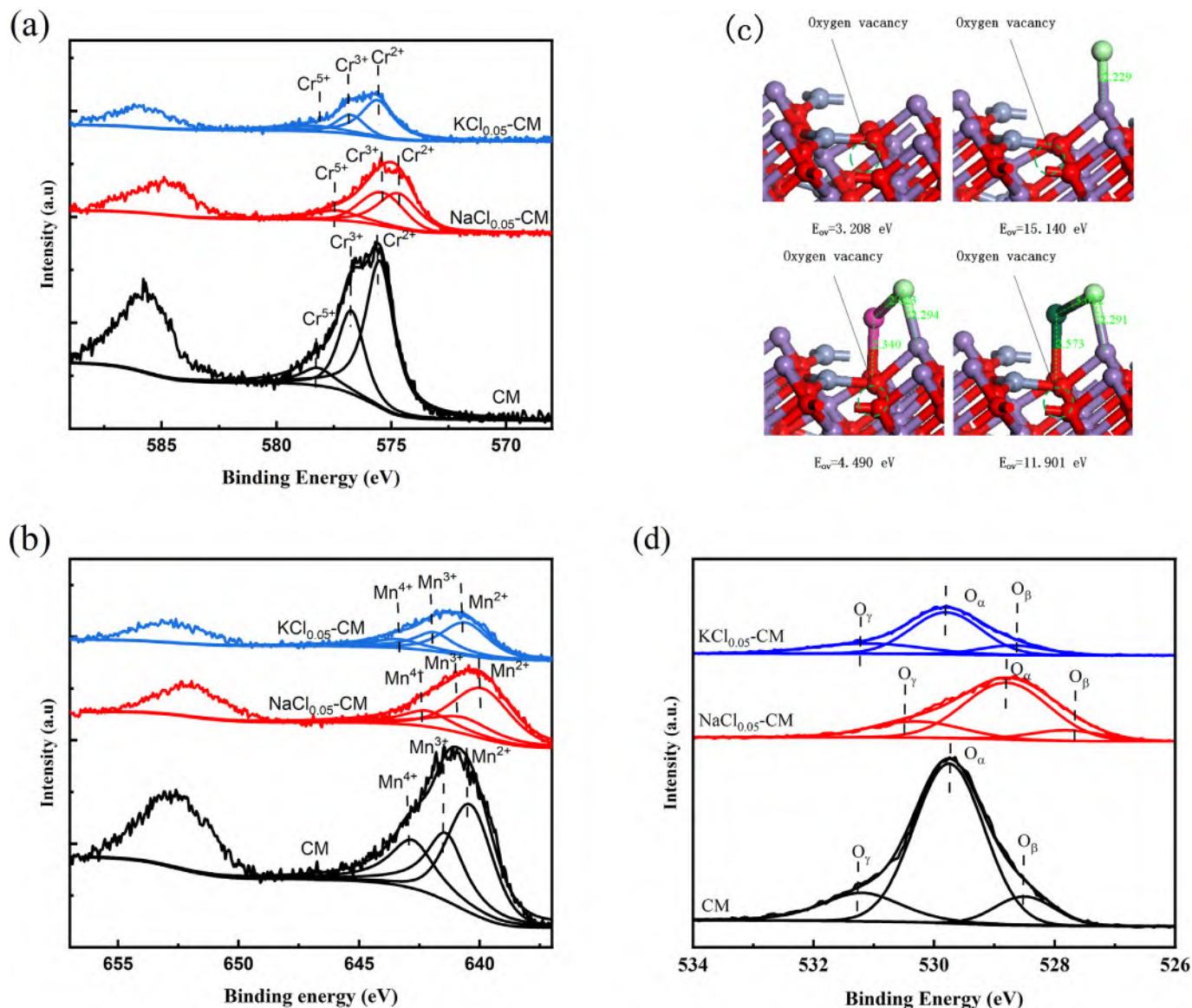


Fig. 3. Cr 2p XPS spectra (a), Mn 2p XPS spectra (b), Optimized structures of oxygen vacancies (c), O 1s XPS spectra (d), O₂-TPD profiles (e), H₂-TPD profiles (f) and optimized structures of alkali metal adsorption (Purple, gray, red, rose red, laurel-green and dark green balls represent Mn, Cr, O, Na, Cl and K, respectively.). (For interpretation of the references to colour in this figure legend, the reader is referred to the web version of this article.)

indicating that the activity of surface adsorbed oxygen ions/surface lattice oxygen for CM is superior to that of other catalysts (Shen et al., 2020). Compared with NaCl_{0.05}-CM catalyst, though intensities of the surface adsorbed oxygen ions/surface lattice oxygen peak were almost same, the bulk lattice oxygen peak of KCl_{0.05}-CM catalyst shifted to higher temperature range, thereby reducing bulk lattice oxygen activity. As a result, it could be safely concluded that both NaCl and KCl could decrease the activity of oxygen species and KCl could cause more severe poisoning on oxygen species than NaCl.

H₂-TPR experiments were carried out to assess the effect of NaCl and KCl on the redox properties of CM catalyst. As shown in Fig. 3f, all H₂-TPR curves consisted of two reduction peaks, which were attributed to the reduction of Mn₃O₄ to MnO (413/450 °C) and Cr₂O₃ to CrO (289/329/385 °C), respectively (Chen et al., 2010; Liu et al., 2020a). After adding NaCl and KCl, the peaks of Cr₂O₃ and Mn₃O₄ shifted higher temperature, indicating that NaCl and KCl could reduce the redox properties (Jiang et al., 2020b). Compared with NaCl_{0.05}-CM catalyst, the Cr₂O₃ peak of KCl_{0.05}-CM catalyst shifted lower temperature, but its total reduction peak area obviously reduced, which might be a reason further decreasing

redox properties. Reduced redox ability of CM catalyst by NaCl and KCl was responsible for well N₂ selectivity.

In this section, the effect of alkali metal adsorption on Mn—O bond of CM catalyst was calculated, and the related models were shown in Fig. 3g. Na and K could adsorb stably on O_{3c} sites with adsorption energy of -2.184 and -2.594 eV, respectively. After Na and K adsorption, vicinal Mn—O bond was enlarged from 2.030 to 2.097 and 2.109 Å, respectively, indicating that Na and K could weaken Mn—O bond due to the electron transfer from Na and K to Mn, which might a vital cause declining the activity of Mn site (Jiang et al., 2021b; Shen et al., 2020). Cl could interact with metal sites including Cr and Mn, and Mn site exhibited lower adsorption energy (-2.482 eV) than Cr site (-1.678 eV), indicating that Mn site shown stronger affinity for Cl than Cr. Compared with Na and K adsorption, Mn—O bond influenced by Cl was weaker due to less change of Mn—O bond length. NaCl and KCl adsorbed on surface exhibited higher adsorption energy than single Na, K and Cl, indicating that the strong interaction between Na/K and Cl could diminish the interaction between Na/K with surface. However, the combination of Na/K and Cl did not alleviate the destruction of Mn—O bond by single Na or K, and it still had a negative effect on Mn—O bond.

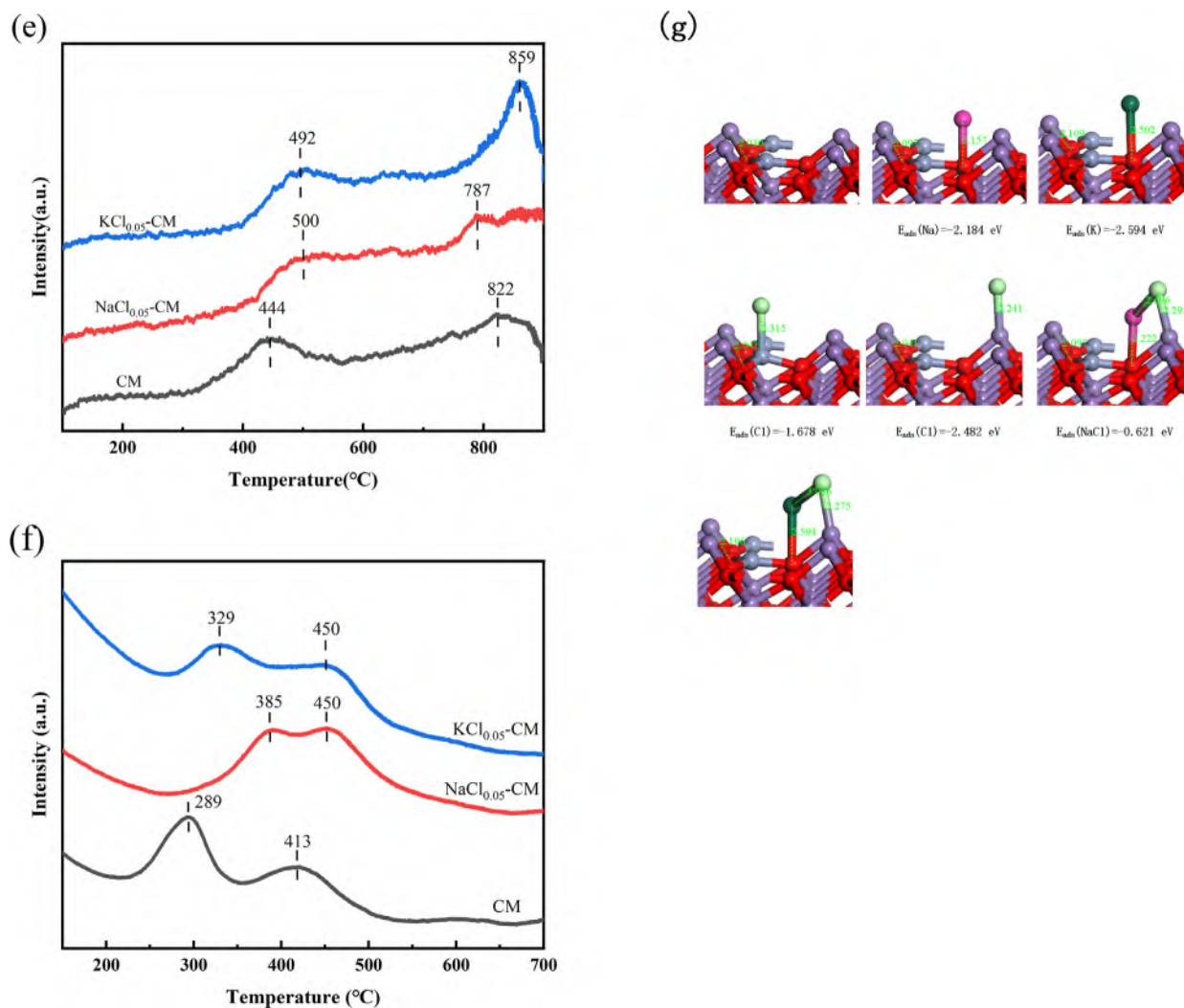


Fig. 3 (continued).

3.4. Surface acidity properties

NH₃-TPD experiments were employed to explore the effect of NaCl and KCl on the surface acidity of CM catalyst. As shown in Fig. 4a, all catalysts possessed one common peak at 95 °C ascribed to NH₄⁺ on Brønsted acid sites (Qin et al., 2022). However, CM catalyst exhibited another new strong peak at 352 °C attributed to coordinated NH₃ on Lewis acid sites (Liu et al., 2020b). After doping NaCl or KCl, Brønsted acid declined obviously and Lewis acid even disappeared, indicating that both NaCl and KCl could strongly interact with acid sites and suppress NH₃ adsorption (Jiang et al., 2020a). The NH₃-TPD peak areas were also calculated based on Fig. 4a and the results were shown in Table 1. The peak areas were ranked by CM > NaCl_{0.05}-CM > KCl_{0.05}-CM, indicating that both NaCl and KCl resulted in serious losses of acidity, and KCl exhibited stronger poison effect on surface acidity than NaCl.

In situ DRIFTS experiments were used to further investigate the effect of NaCl and KCl on surface acidity. For CM catalyst (Fig. 4b), several bands at 1200–1222, 1255, 1290, 1440, 1515, 1600, 1641, 3133–3376 cm⁻¹ were detected. The bands at 1200–1222, 1255, 1290, 1600 cm⁻¹ were attributed to NH₃ coordinated to Lewis acid sites (Xue et al., 2021; Yu et al., 2021). The bands at 1440/1641 cm⁻¹ were ascribed to NH₄⁺ ion bound to Brønsted acid sites (Zeng et al., 2020). The band at 1515 cm⁻¹ was -NH₂ species due to the oxidation and decomposition of adsorbed NH₃ (Tan et al., 2020). Other bands at above 3100 cm⁻¹ were related to the N–H bond stretching vibration of adsorbed NH₃ (Zhang et al., 2021). It

could be observed that CM catalyst was dominated by abundant Lewis acid and Brønsted acid, and the amount of Brønsted acid was higher than Lewis acid at below 120 °C. However, with increasing temperature, Brønsted acid declined rapidly and hardly vanished at 120 °C, but Lewis acid almost changed, suggesting that Lewis acid was more stable than Brønsted acid (Huang et al., 2021). Furthermore, CM catalyst could exhibit excellent NH₃-SCR activity above 120 °C. Consequently, Lewis acid sites were responsible for its excellent NH₃-SCR activity. The bands at 1600 and 1641 cm⁻¹ exhibited the opposite trend from 30 to 120 °C, suggesting that some Lewis acid could be formed from the decomposition of unable Brønsted acid.

In situ DRIFTS of NH₃ adsorption over NaCl_{0.05}-CM and KCl_{0.05}-CM catalysts were shown in Fig. 4c-d. The bands at 1436, 1627 and 1631 cm⁻¹ were attributed to NH₄⁺ on Brønsted acid sites. The bands at 1544 and 1608 cm⁻¹ were related to -NH₂ species and coordinated NH₃ on Lewis acid sites, respectively. It was obvious that after NaCl and KCl addition, NH₃ adsorption peak intensities obviously decreased. With increasing temperature, Brønsted acid and Lewis acid of NaCl_{0.05}-CM and KCl_{0.05}-CM catalysts disappeared rapidly, indicating that NaCl and KCl significantly reduced the stability of Brønsted/Lewis acid. As a result, NaCl and KCl could not only obviously inhibit NH₃ adsorption, but also weaken the thermal stability of adsorbed NH₃ species.

In this section, we further investigated NH₃ adsorption with the purpose of figuring out alkali effect on surface Lewis acid. As shown in Fig. 4e, Mn exhibited lower adsorption energy (-1.325 eV) for NH₃ in comparison

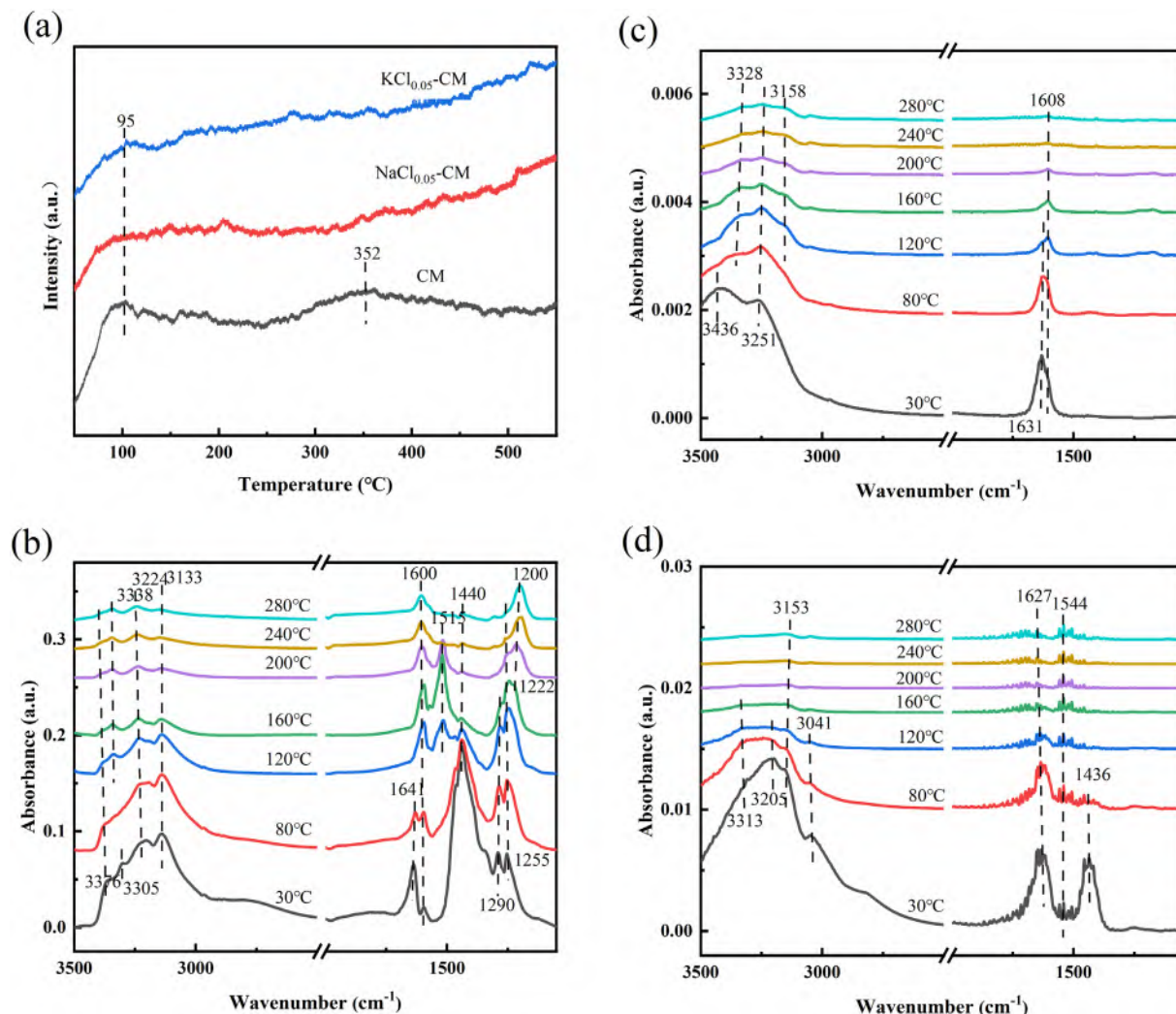


Fig. 4. NH_3 -TPD profiles (a), *in situ* DRIFTS spectra of NH_3 adsorption over CM (b), $\text{NaCl}_{0.05}\text{-CM}$ (c) and $\text{KCl}_{0.05}\text{-CM}$ (d) catalysts and optimized structures of NH_3 (e) and NH_4^+ (f) adsorption.

with Cr (-0.747 eV), indicating that Mn as main Lewis acid sites took part in NH_3 -SCR reactions. After Na and K addition, the NH_3 adsorption energy on Mn site increased to -1.235 and -1.079 eV, respectively, demonstrating that both Na and K could slightly suppress NH_3 adsorption and decrease Lewis acid, and K had stronger inhibiting effect on Lewis acid formation than Na. However, compared with NH_3 adsorption, Cl showed stronger combining capacity with Mn (-2.482 eV), demonstrating that competitive adsorption between NH_3 and Cl on Mn site was a main reason reducing Lewis acid instead of Na and K. After NaCl and KCl introduction, KCl exhibited stronger inhibiting effect on Lewis acid formation than NaCl, but the poisoning effect of NaCl and KCl on Lewis acid was still weaker than single Na and K due to the strong interaction between Na/K and Cl.

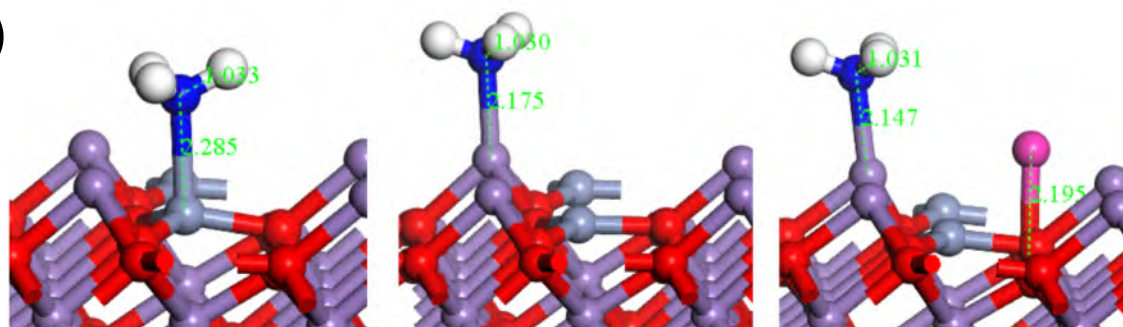
NH_3 adsorbed on Brønsted acid sites (O site) in the form of NH_4^+ , which was significant intermediate in NH_3 -SCR reactions following L-H mechanism. As shown in Fig. 4f, NH_4^+ adsorb on O_{3c} exhibited lower adsorption energy (-3.365 eV) than Na and K on O_{3c} , indicating that O_{3c} exhibited stronger affinity to NH_4^+ instead of Na or K and Brønsted acid formation was not influenced by the competitive adsorption between Na/K and NH_4^+ on O_{3c} . After Cl addition, it was clear that NH_4^+ adsorption energy obviously decreased, indicating that Cl adsorption was unfavorable for Brønsted acid formation. NaCl and KCl exhibited almost same adsorption energy for NH_4^+ as Cl, illustrating that the interaction between Na/K and Cl hardly changed the negative effect of Cl on Brønsted acid.

3.5. Surface NO_x adsorption properties

In situ DRIFTS of $\text{NO} + \text{O}_2$ adsorption was used to explore the effect of NaCl and KCl on the formation of surface nitrates, and related results were shown in Fig. 5. For CM catalyst (Fig. 5a), several bands at 1205, 1434 and 1633 cm^{-1} were attributed to NO^- (Wei et al., 2018), linear nitrite (Liu et al., 2021d) and adsorbed NO_2 (Pan et al., 2021b), respectively. The bands at 1295 and 1612 cm^{-1} belonged to monodentate nitrate (Nam et al., 2021; Wei et al., 2021). The bands at 1544 and 1569 cm^{-1} were ascribed to bidentate nitrate (Wang et al., 2021). Other bands at 1253, 1268 and 1353 cm^{-1} were related to bridged nitrate (Shi et al., 2021; Wu et al., 2021). Monodentate nitrate (1295 cm^{-1}) vanished with increasing temperature, but new band at 1253 and 1268 cm^{-1} arose, suggesting that monodentate nitrate was very unstable and could be easily converted into bridged nitrate. Similarly, the same phenomenon happened in the bands at 1434, 1544 and 1569 cm^{-1} , suggesting that unstable linear nitrate could be converted into bidentate nitrate. As reaction temperature increased to 160 $^\circ\text{C}$, a new band (1633 cm^{-1}) emerged and remained stability above 160 $^\circ\text{C}$, perhaps it was due to the continuous decomposition of monodentate nitrate.

In situ DRIFTS of $\text{NO} + \text{O}_2$ adsorption over $\text{NaCl}_{0.05}\text{-CM}$ and $\text{KCl}_{0.05}\text{-CM}$ were shown in Fig. 5b-c, respectively. The bands at 1263 and 1376 cm^{-1} were related to bridged nitrate. The bands at 1427 and 1612 cm^{-1}

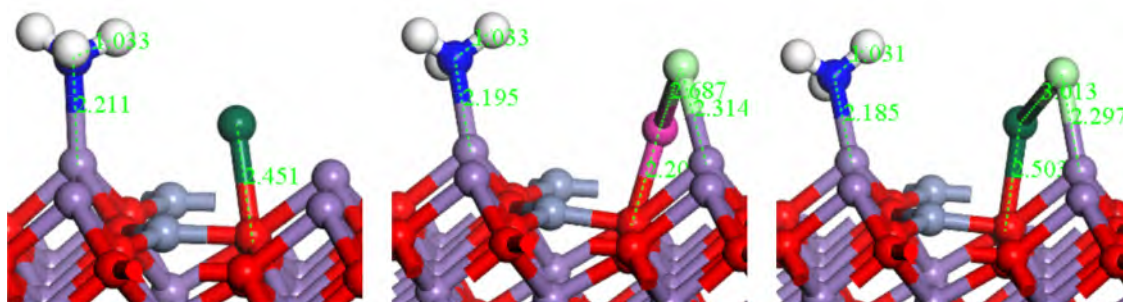
(e)



$E_{\text{ads}}(\text{NH}_3) = -0.747 \text{ eV}$

$E_{\text{ads}}(\text{NH}_3) = -1.325 \text{ eV}$

$E_{\text{ads}}(\text{NH}_3) = -1.235 \text{ eV}$

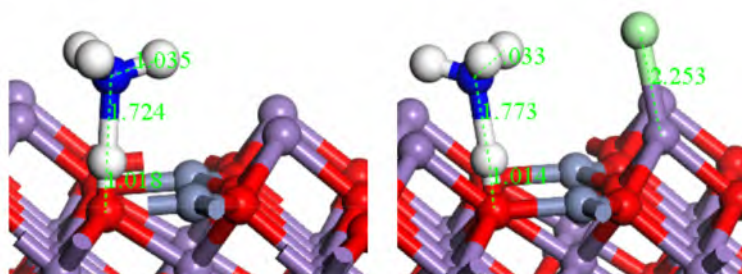


$E_{\text{ads}}(\text{NH}_3) = -1.079 \text{ eV}$

$E_{\text{ads}}(\text{NH}_3) = -1.285 \text{ eV}$

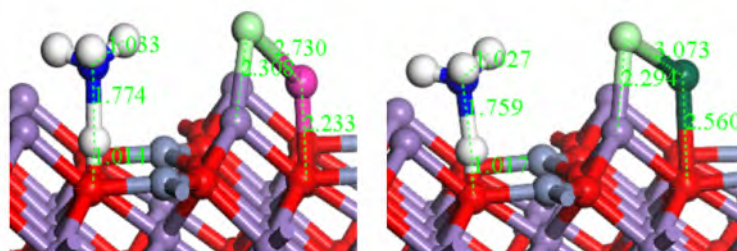
$E_{\text{ads}}(\text{NH}_3) = -1.150 \text{ eV}$

(f)



$E_{\text{ads}}(\text{NH}_4^+) = -3.365 \text{ eV}$

$E_{\text{ads}}(\text{NH}_4^+) = -2.828 \text{ eV}$



$E_{\text{ads}}(\text{NH}_4^+) = -2.791 \text{ eV}$

$E_{\text{ads}}(\text{NH}_4^+) = -2.748 \text{ eV}$

Fig. 4 (continued).

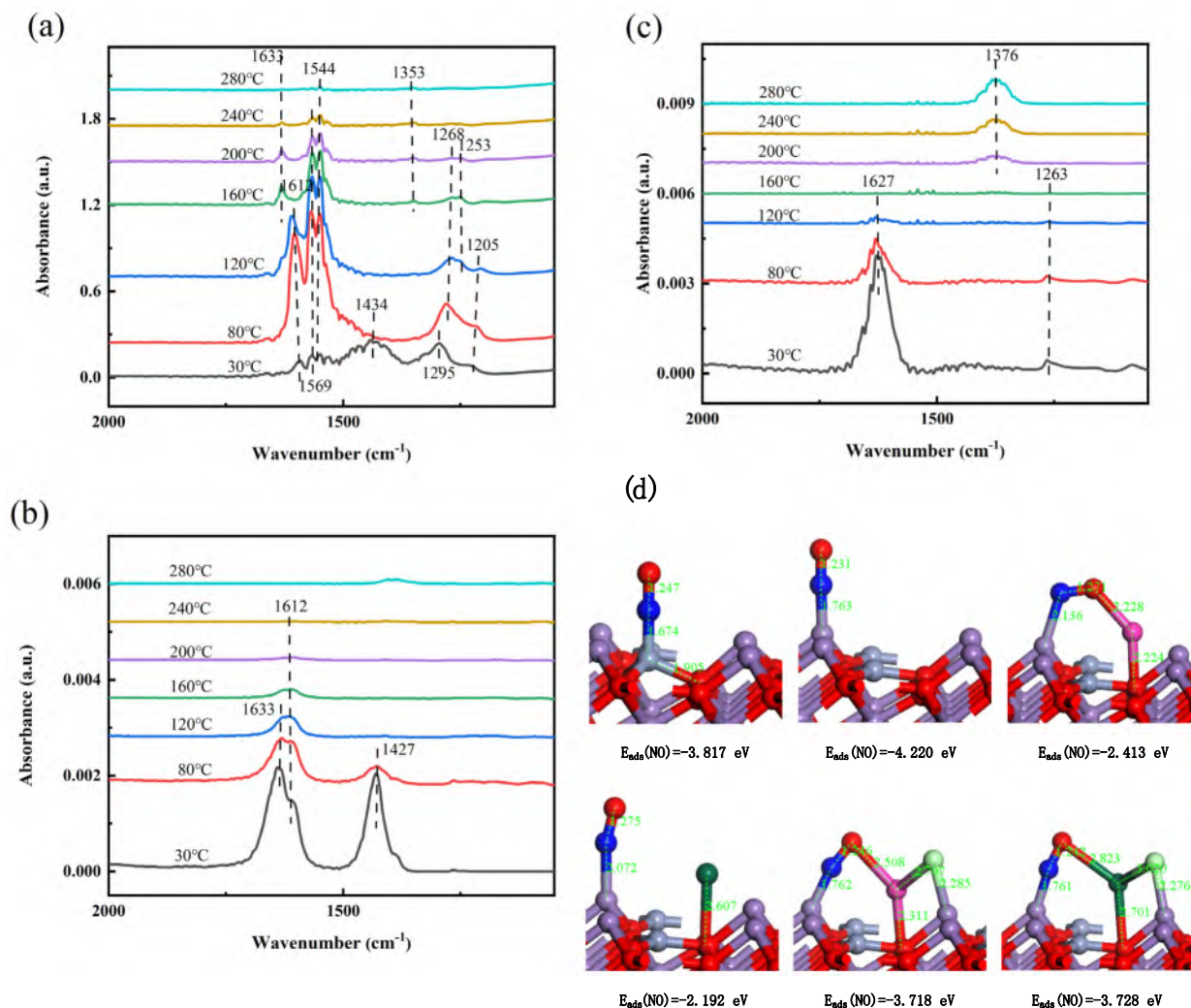


Fig. 5. *In situ* DRIFTS spectra of NO + O₂ co-adsorption over CM (a), NaCl_{0.05}-CM (b) and KCl_{0.05}-CM (c) catalysts and optimized structures of NO adsorption (d).

belonged to linear nitrite and monodentate nitrate, respectively. The bands at 1627 and 1633 cm⁻¹ were attributed adsorbed NO₂. With increasing temperature, all NO_x species except new band (1376 cm⁻¹) faded away. Compared with CM catalyst, NaCl and KCl obviously suppressed NO_x species adsorption and weakened their stability due to the interaction between NaCl/KCl and active sites, thereby inhibiting the formation of surface nitrates.

NO adsorption and activation influenced by NaCl and KCl were further investigated by DFT calculations. As shown in Fig. 5d, NO adsorption energy on Mn and Cr sites was -4.220 and -3.817 eV, respectively. Hence, Mn exhibited stronger affinity for NO than Cr. After Na and K addition, Na and K could weaken Mn—N bond, demonstrating that both Na and K could suppress NO adsorption/activation and hinder the formation of surface adsorbed NO₂ and nitrates. Compared with K effect, Na had weaker inhibiting effect on NO adsorption due to Na—O bond formation. With Cl further introduction, the poisoning effect of Na and K was ulteriorly receded, indicating that the interaction between Na/K and Cl could weaken the poisoning effect of Na and K on surface NO_x species.

3.6. Reaction mechanism

Transient reaction experiment was carried out to investigate the effect of NaCl and KCl on the reaction mechanism. For CM catalyst (Fig. 6a), after N₂ purge for 30 min, it was clear that abundant acid sites existed in CM catalyst, including Brønsted acid (1440 cm⁻¹), Lewis acid (1222 and 1600 cm⁻¹). In addition, -NH₂ species (1515 cm⁻¹) and adsorbed NH₃

species (3143–3384 cm⁻¹) could also be observed. With increasing time, NH₃ adsorption bands gradually weakened and even disappeared, and NO_x species still didn't emerge, indicating that adsorbed NH₃ could constantly react with gaseous NO. Consequently, NH₃-SCR reaction over CM catalyst complied with *Eley-Rideal* (*E-R*) mechanism (Jiang et al., 2021a). With increasing reaction time, new bands at 1253, 1544, 1569 and 1612 cm⁻¹ ascribed to bridged nitrate, bidentate nitrate, bidentate nitrate and monodentate nitrate, respectively, were observed. As time went by, their intensities gradually increased and adsorbed NO₂ (1633 cm⁻¹) was gradually formed from the decomposition of monodentate nitrate.

As for NaCl_{0.05}-CM catalyst (Fig. 6b) and KCl_{0.05}-CM catalyst (Fig. 6c), after N₂ purge for 30 min, it was clear that the bands at 1400 and 1627 cm⁻¹ were ascribed to NH₄⁺ on Brønsted acid sites, and the band at 1608 cm⁻¹ was related to coordinated NH₃ on Lewis acid sites. Compared with CM catalyst, the intensities of NH₃ adsorption bands over NaCl_{0.05}-CM and KCl_{0.05}-CM catalyst distinctly declined, indicating that NaCl and KCl were unfavorable for NH₃ adsorption/activation. For NaCl_{0.05}-CM catalyst, the bands never changed with increasing time, indicating that adsorbed NH₃ species were inactivated and not reacted with gaseous NO. Hence, NaCl cut off NH₃-SCR reactions following *E-R* mechanism. But for KCl_{0.05}-CM catalyst, the peak at 1400 cm⁻¹ attributed to NH₄⁺ on Brønsted acid sites vanished after purging NO + O₂ for 5 min, and then new band at 1380 cm⁻¹ ascribed to bridged nitrate was observed, indicating that some NH₃-SCR reactions between adsorbed NH₃ and gaseous NO existed. However, the peak intensities of Lewis acid at 1627 cm⁻¹ almost unchanged, indicating that it cut off “Fast-SCR” reactions by inactivating

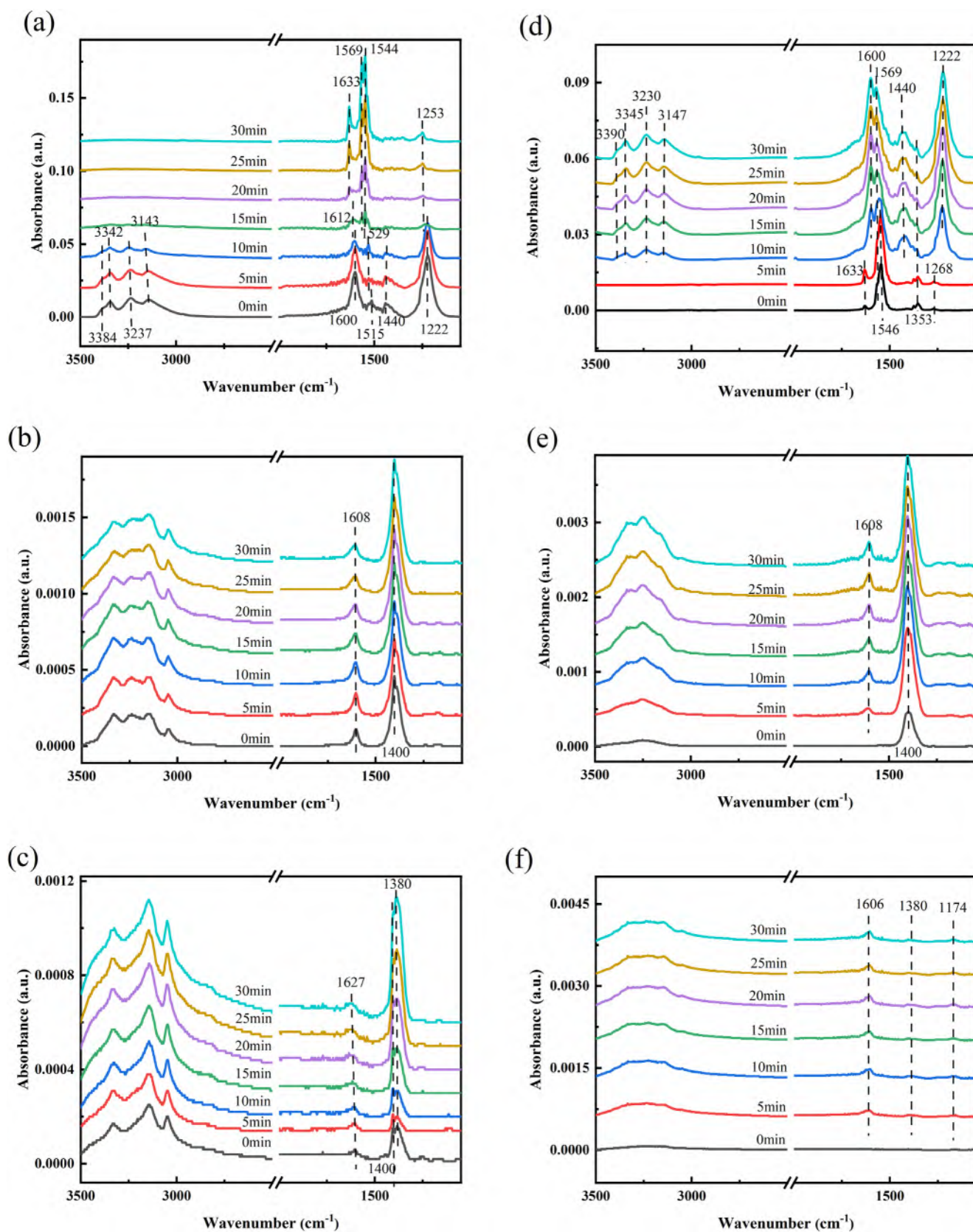


Fig. 6. *In situ* DRIFTS reactions between NO + O₂ and pre-adsorbed NH₃ over CM (a), NaCl_{0.05}-CM (b) and KCl_{0.05}-CM (c) catalysts at 160 °C, between NH₃ and pre-adsorbed NO + O₂ species over CM (d), NaCl_{0.05}-CM (e) and KCl_{0.05}-CM (f) catalysts at 160 °C and between NH₃ + NO + O₂ species over CM (g), NaCl_{0.05}-CM (h) and KCl_{0.05}-CM (i) catalysts.

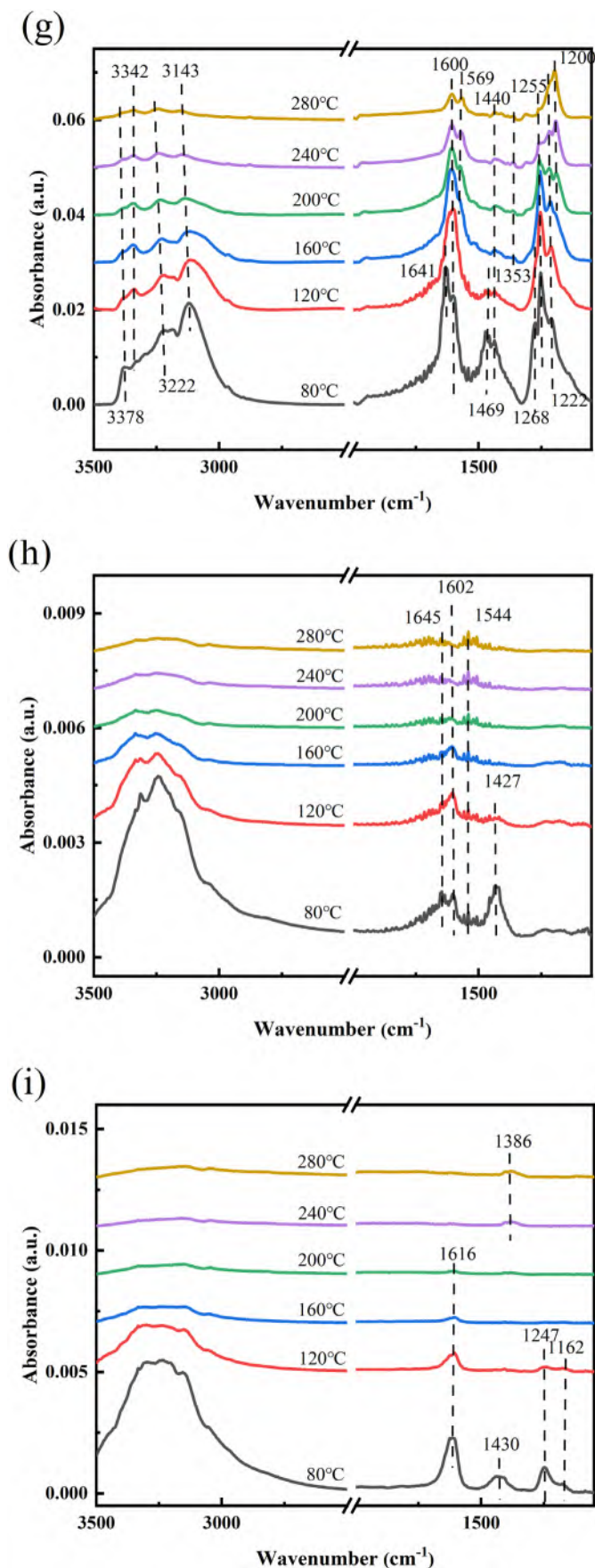


Fig. 6 (continued).

Lewis acid by KCl and KCl. As a result, KCl could weaken NH_3 adsorption, but not change E-R mechanism of NH_3 -SCR reactions.

Transient reaction experiment between pre-adsorbed $\text{NO} + \text{O}_2$ and NH_3 was carried out to further investigate the effect of NaCl and KCl on reaction mechanism, and the results were shown in Fig. 6. For CM catalyst (Fig. 6d), several bands at 1268/1353, 1544/1569 and 1633 cm^{-1} were attributed to bridged nitrate bands, bidentate nitrate bands and adsorbed NO_2 band (1633 cm^{-1}) after $\text{NO} + \text{O}_2$ purging for 30 min. It was clear that the intensities of bands (1546, 1549 and 1633 cm^{-1}) increased with increasing time owing to the overlap of $\text{NH}_4^+/-\text{NH}_2$ and adsorbed NO_x species, respectively, indicating that adsorbed NO_x species was insert and could not interact with gaseous NO rapidly. As time increased to 10 min, bridged nitrate (1268 cm^{-1}) and adsorbed NO_2 faded away, suggesting that some NH_3 -SCR reactions between adsorbed NO_x and NH_3 species happened. Hence, CM catalyst followed *Langmuir-Hinshelwood* (L-H) mechanism (Wu et al., 2019).

As for $\text{NaCl}_{0.05}$ -CM catalyst (Fig. 6e), there was only one band at 1400 cm^{-1} ascribed to linear nitrite after N_2 purge for 30 min. With increasing time, new band at 1608 cm^{-1} belonged to coordinated NH_3 on Lewis acid sites was observed, and the band at 1400 cm^{-1} originated from the overlap of NH_4^+ and linear nitrite, indicating that some reactions between adsorbed NO_x species and NH_3 species took place. Consequently, NaCl did not change L-H mechanism reactions of CM catalyst. But for $\text{KCl}_{0.05}$ -CM catalyst (Fig. 6f), there was no band after N_2 purge for 30 min because KCl seriously suppressed the formation of adsorbed NO_x species.

$\text{NH}_3 + \text{NO} + \text{O}_2$ adsorption was carried out to further investigate the effect of NaCl and KCl on reaction mechanism during NH_3 -SCR reactions. For CM catalyst (Fig. 6g), the bands at 1200/1222/1255/1600 and 1440/1469/1641 cm^{-1} were related to coordinated NH_3 on Lewis acid sites and NH_4^+ on Brønsted acid sites, respectively. Other bands at 1268/1353 and 1569 cm^{-1} were related to bridged nitrate and bidentate nitrate, respectively. In all temperature range, both active bidentate nitrate and bridged nitrate could interact with adsorbed NH_3 species, thereby demonstrating that NH_3 -SCR reactions over CM catalyst adhered to L-H mechanism. Furthermore, active adsorbed NH_3 species could combine with gaseous NO . Consequently, NH_3 -SCR reactions over CM catalyst also followed E-R mechanism.

For $\text{NaCl}_{0.05}$ -CM catalyst (Fig. 6h), the bands at 1427, 1544, 1602 and 1645 cm^{-1} were ascribed to linear nitrite, $-\text{NH}_2$ species, coordinated NH_3 and NH_4^+ , respectively. Adsorbed NO_x species interacted with adsorbed NH_3 species. It was demonstrated that NH_3 -SCR reactions over $\text{NaCl}_{0.05}$ -CM catalyst complied with L-H mechanism. As for $\text{KCl}_{0.05}$ -CM catalyst (Fig. 6i), the bands at 1162, 1430, 1247 and 1616 cm^{-1} were attributed to coordinated NH_3 , NH_4^+ , bridged nitrate and monodentate nitrate, respectively. With increasing temperature, new band at 1386 cm^{-1} attributed to bridged nitrate could be observed. NH_3 -SCR reactions between adsorbed NH_3 and NO_x species existed, and NH_3 -SCR reactions over $\text{KCl}_{0.05}$ -CM catalyst complied with L-H mechanism. Moreover, active adsorbed NH_3 species combined with gaseous NO , thereby also demonstrating that NH_3 -SCR reactions over $\text{KCl}_{0.05}$ -CM catalyst also complied with E-R mechanism.

3.7. Reaction steps

3.7.1. E-R mechanism

According to the calculated results of NH_3 adsorption, NH_3 could stably adsorb on Mn site. Accordingly, NH_3 -SCR reaction pathways (E-R mechanism) over CM catalyst were calculated, and the related models and reaction energy profile were shown in Fig. 7a-b. NH_3 adsorption/decomposition was the first step in simulating E-R mechanism reactions. NH_3 molecule anchored in Mn site by its N atom to form a stable intermediate structure (denoted as IM1). Soon afterwards, one H atom of NH_3 molecule moved to nearby location, and NH_2 group was close to Mn atom to form the second intermediate structure, namely IM2. In IM2, N—Mn bond shrank from 2.175 to 1.935 Å. The reaction step (IM1 to IM2) was endothermic by 0.123 eV and need to overcome 2.383 eV energy barrier to reach transition state (TS1). Gaseous NO molecule was gradually close to

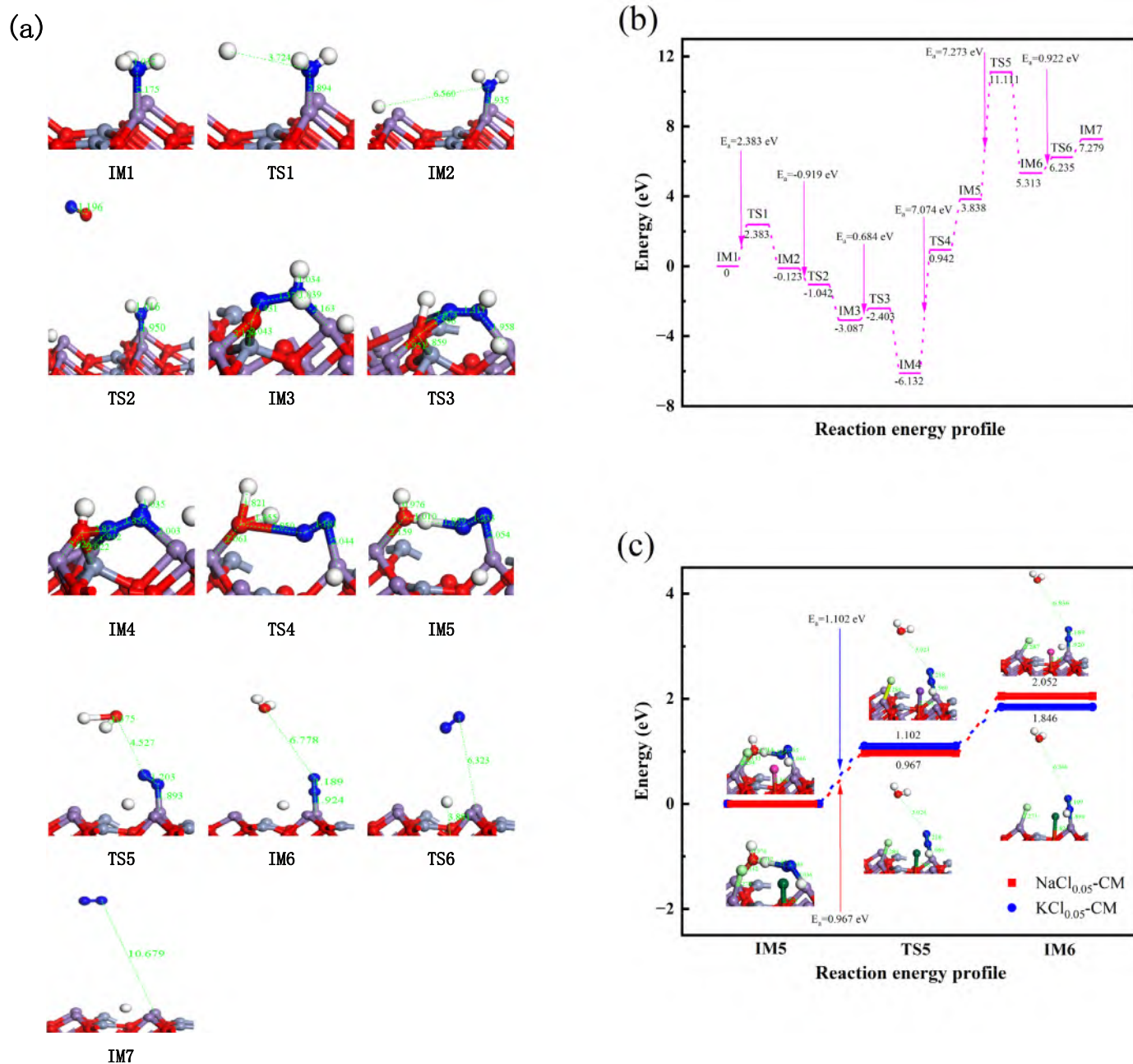


Fig. 7. Reaction pathways of N₂ formation (a), reaction energy profile (b) and reaction energy profile influenced by NaCl and KCl (c) during E-R mechanism reactions. Reaction pathways of N₂ formation (d), reaction energy profile (e) and reaction energy profile influenced by NaCl and KCl (f) during L-H mechanism reactions.

NH₂ group to form ONNH₂ intermediate, namely IM3. In IM3, O atom of NO was connected to Mn atom and Cr atom, and N—Mn bond was further enlarged from 1.935 to 2.163 Å. This process (IM2 → TS2 → IM3) was endothermic by 2.964 eV, corresponding to -0.919 eV energy barrier (TS2), indicating that this process was spontaneous. ONNH₂ intermediate was continually dehydrogenated one H atom and converted into HONNH intermediate (IM4). In this process (IM3 to IM4), one H atom of NH₂ transferred and combined with O atom of ON. The transfer step of related H atom was endothermic by 3.045 eV, corresponding to energy barrier (TS3) of 0.648 eV. Based on IM4, the N—O and N—H bonds of HONNH intermediate ruptured, and one H atom was transferred to connect to O atom and another N atom to form stable H₂ONN intermediate (IM5). This isomerization process was endothermic by 9.97 eV and need to overcome 7.074 eV energy barrier to reach TS4. Subsequently, N—H bond and Mn—O bond was broken, and H₂O of H₂ONN intermediate based on IM5 was gradually away from the matrix to form IM6. In this process (IM5 → TS5 → IM6), H₂O

desorption was endothermic by 1.375 eV, corresponding to 7.273 eV energy barrier. Eventually, Mn—N bond gradually ruptured until N₂ desorption to form the next intermediate (IM7). In the process of IM6 → TS6 → IM7, N₂ desorption was endothermic by 1.966 eV and need to overcome 0.922 eV energy barrier to climb TS6. It was obvious that the energy barrier of H₂O desorption process (IM5 → TS5 → IM6) was the highest, indicating that H₂O desorption was the rate-controlling step of NH₃-SCR reaction that followed E-R mechanism (Fang et al., 2019b). The effect of alkali on this rate-controlling step was further investigated, and the results were shown in Fig. 7c. In IM5, Na (K) and Cl could stably adsorb on O_{3c} and Mn site, respectively, and O atom of OH₂N₂ was connected to another Mn site and one H of OH₂N₂ was closed to N atom of OH₂N₂ to form a stable intermediate (IM5). Soon afterwards, O—Mn and N—H bonds were broken and H₂O gradually escaped from the matrix to form the next intermediate (IM6). This rate-controlling process was endothermic by 2.052 (NaCl_{0.05}-CM) and 1.846 eV (KCl_{0.05}-CM),

One H atom of formed NH_2NO structure in IM4 continually escaped and gradually approached to one O atom of NH_2NO to form NHNOH structure (IM5), which was endothermic by 0.122 eV and overcome 2.153 eV barrier energy. Based on IM5, $\text{O}_{3c}\text{-H-N}$ bond was gradually enlarged and broken, and N atom of NNOH got one H atom from O-H bond, then O-N bond was broken and O attracted two H atom to form one H_2O molecule. In the process of H_2O formation ($\text{IM5} \rightarrow \text{TS5} \rightarrow \text{IM6}$), the reaction was exothermic by 1.726 eV and the reaction energy was 1.928 eV. Soon afterwards, H_2O and N_2 was desorbed one by one to form IM7 and IM8, which was endothermic by 2.837 and 3.175 eV, corresponding to energy barrier of 6.085 and 0.875 eV, respectively. It was obvious that the reaction energy barrier of H_2O desorption process ($\text{IM6} \rightarrow \text{TS6} \rightarrow \text{IM7}$) was the highest, indicating that H_2O desorption was also the rate-controlling step of $\text{NH}_3\text{-SCR}$ reaction that followed L-H mechanism. The effect of alkali on this rate-controlling step was further investigated, and the results were shown in Fig. 7f. In IM6, Na (K) and Cl could stably adsorb on O_{3c} and Mn site, respectively, and O atom of H_2O was closed to one N atom of N_2 on Mn site to form a stable intermediate (IM6). Soon afterwards, the distance between N and O atoms gradually enlarged and H_2O gradually escaped from the matrix to form the next intermediate (IM7). This rate-controlling process was endothermic by -0.089 ($\text{NaCl}_{0.05}\text{-CM}$) and 0.931 eV ($\text{KCl}_{0.05}\text{-CM}$), corresponding to energy barrier of 1.091 and 7.547 eV that had to overcome, respectively. Compared with CM catalyst, NaCl not only decreased reaction heat of rate-controlling step, but also reduce its reaction energy barrier, indicating that reaction energy barrier and reaction heat were not reasons poisoning CM catalyst by NaCl. Compared with CM catalyst, though KCl reduced its reaction heat of rate-controlling step, but increased its reaction energy barrier. It indicated that reaction energy barrier of rate-controlling step might be a vital reason poisoning CM catalysts by KCl in $\text{NH}_3\text{-SCR}$ reactions that followed L-H mechanism.

4. Conclusions

In summary, we successfully illustrated the poisoning mechanism of CM catalyst by alkali metals by experiments and DFT calculations. The characterizations unveiled that NaCl and KCl could make a decrease in specific surface area, electron transfer ($\text{Cr}^{5+} + \text{Mn}^{3+} \leftrightarrow \text{Cr}^{3+} + \text{Mn}^{4+}$), redox ability, oxygen vacancies formation, NH_3 adsorption, the stability of Brønsted/Lewis acid and surface NO_x species variety, amount and stability. Furthermore, NaCl cut off E-R mechanism by inactivating surface Brønsted/Lewis acid. DFT calculations revealed that Na and K could weaken Mn—O bond, competitive adsorption between Cl and NH_3 on Mn site was a main reason weakening surface Lewis acid and Cl adsorption was major reason diminishing Brønsted acid and oxygen vacancies. Both Na and K had an obvious inhibition effect on NO adsorption/activation. NaCl and KCl increased reaction heat of rate-controlling step (H_2O desorption) in E-R mechanism reactions and KCl elevated its energy barrier in L-H mechanism reactions, which might be vital reasons poisoning CM catalyst. However, it is still a challenge to design SCR catalysts with excellent alkali metal resistance. Based above research results, it is expected that SCR catalysts with excellent alkali metal resistance can be designed by setting up a cage to trap Cl atom to release Mn site, thereby recovering surface acidity and oxygen vacancies. In addition, doping some metal elements with abundant active sites to make up for a loss of surface acidity and adsorbed NO_x species is also good strategy.

Conventional cell and (111) facet of $\text{CrMn}_{1.5}\text{O}_4$; N_2 selectivity.

CRedit authorship contribution statement

Ninghan Wei: Conceptualization, Investigation, Methodology, Writing original draft. **Xiaomei Hu:** Investigation, Methodology. **Cheng Zhao:** Conceptualization, Methodology, Validation. **Zhangfa Tong:** Formal analysis, Validation. **Junge Yun:** Formal analysis. **Xueying Jiang:** Formal analysis. **Keju Wang:** Investigation. **Yun Zou:** Conceptualization, Supervision,

Writing, Review and editing. **Zhihang Chen:** Conceptualization, Funding acquisition, Supervision, Writing, Review and Editing.

Data availability

No data was used for the research described in the article.

Declaration of competing interest

The authors declare that they have no known competing financial interests or personal relationships that could have appeared to influence the work reported in this paper.

Acknowledgments

This work was financially supported by Nature Science Foundations of China (21978174), the Science and Technology Program of Guangzhou (201904020038), 2020 Key Projects of Science and Technology Supporting Economy of China (SQ2020YFF0426321), the Central Research Institutes of Basic Research Program, China (PM-zx703-202104-073).

References

- Chen, Z., Li, X., Gao, X., Jiang, Y., Lü, Y., Wang, F., Wang, L., 2009. Selective catalytic reduction of NO_x with NH_3 on a Cr-Mn mixed oxide at low temperature. *Chin. J. Catal.* 30, 4–6.
- Chen, Z., Yang, Q., Li, H., Li, X., Wang, L., Chi Tsang, S., 2010. Cr-MnOx mixed-oxide catalysts for selective catalytic reduction of NO_x with NH_3 at low temperature. *J. Catal.* 276, 56–65.
- Choi, K.-H., Lee, D.-H., Kim, H.-S., Yoon, Y.-C., Park, C.-S., Kim, Y.H., 2016. Reaction characteristics of precious-metal-free ternary Mn-Cu-M (M = Ce, Co, Cr, and Fe) oxide catalysts for low-temperature CO oxidation. *Ind. Eng. Chem. Res.* 55, 4443–4450.
- Fang, D., He, F., Xie, J., 2019a. Characterization and performance of common alkali metals and alkaline earth metals loaded Mn/TiO₂ catalysts for NO_x removal with NH_3 . *J. Energy Inst.* 92, 319–331.
- Fang, Q., Zhu, B., Sun, Y., Zhu, Z., Xu, M., Ge, T., 2019b. Mechanistic insight into the selective catalytic reduction of NO by NH_3 over $\alpha\text{-Fe}_2\text{O}_3$ (001): a density functional theory study. *Catal. Sci. Technol.* 9, 116–124.
- Gao, F., Tang, X., Yi, H., Zhao, S., Wang, J., Gu, T., 2019. Improvement of activity, selectivity and H_2O & SO_2 -tolerance of micro-mesoporous CrMn_2O_4 spinel catalyst for low-temperature $\text{NH}_3\text{-SCR}$ of NO_x . *Appl. Sur. Sci.* 466, 411–424.
- Gao, E., Huang, B., Zhao, Z., Pan, H., Zhang, W., Li, Y., Bernards, M.T., He, Y., Shi, Y., 2020a. Understanding the co-effects of manganese and cobalt on the enhanced SCR performance for MnxCr_xO_4 spinel-type catalysts. *Catal. Sci. Technol.* 10, 4752–4765.
- Gao, E., Sun, G., Zhang, W., Bernards, M.T., He, Y., Pan, H., Shi, Y., 2020b. Surface lattice oxygen activation via Zr^{4+} cations substituting on A2+ sites of MnCr_2O_4 forming $\text{ZrxCr}_x\text{Mn}_{1-x}\text{-xCr}_2\text{O}_4$ catalysts for enhanced $\text{NH}_3\text{-SCR}$ performance. *Chem. Eng. J.* 380, 122397.
- Hou, Y., Wang, J., Li, Q., Liu, Y., Bai, Y., Zeng, Z., Huang, Z., 2021. Environmental-friendly production of FeNbTi catalyst with significant enhancement in SCR activity and SO_2 resistance for NO_x removal. *Fuel* 285, 119133.
- Huang, X., Dong, F., Zhang, G., Guo, Y., Tang, Z., 2021. A strategy for constructing highly efficient yolk-shell Ce@Mn@TiO_x catalyst with dual active sites for low-temperature selective catalytic reduction of NO with NH_3 . *Chem. Eng. J.* 419, 129572.
- Jiang, Y., Lai, C., Li, Q., Gao, W., Yang, L., Yang, Z., Lin, R., Wang, X., Zhu, X., 2020a. The poisoning effect of KCl and K_2O on $\text{CeO}_2\text{-TiO}_2$ catalyst for selective catalytic reduction of NO with NH_3 . *Fuel* 280, 118638.
- Jiang, Y., Shi, W., Lai, C., Gao, W., Yang, L., Yu, X., Yang, Z., Lin, R., 2020b. The deactivation effect of Na_2O and NaCl on $\text{CeO}_2\text{-TiO}_2$ catalysts for selective catalytic reduction of NO with NH_3 . *J. Energy Inst.* 93, 1332–1340.
- Jiang, B., Zhao, S., Wang, Y., Wenren, Y., Zhu, Z., Harding, J., Zhang, X., Tu, X., Zhang, X., 2021a. Plasma-enhanced low temperature $\text{NH}_3\text{-SCR}$ of NO_x over a Cu-Mn/SAPO-34 catalyst under oxygen-rich conditions. *Appl. Catal. B-Environ.* 286, 119886.
- Jiang, Y., Liu, T., Lai, C., Yang, Z., Lin, R., Wang, X., Zhu, X., 2021b. Deactivation of $\text{CeO}_2\text{-TiO}_2$ catalyst by K_2SO_4 for $\text{NH}_3\text{-SCR}$: an experimental and DFT study. *Appl. Sur. Sci.* 547, 149196.
- Li, Q., Li, X., Li, W., Zhong, L., Zhang, C., Fang, Q., Chen, G., 2019a. Effect of preferential exposure of anatase TiO_2 0 0 1 facets on the performance of Mn-Ce/TiO₂ catalysts for low-temperature selective catalytic reduction of NO_x with NH_3 . *Chem. Eng. J.* 369, 26–34.
- Li, X., Li, Q., Zhong, L., Song, Z., Yu, S., Zhang, C., Fang, Q., Chen, G., 2019b. DFT analysis of the reaction mechanism for $\text{NH}_3\text{-SCR}$ of NO_x over Mn/ $\gamma\text{-Al}_2\text{O}_3$ catalyst. *J. Phys. Chem. C* 123, 25185–25196.
- Li, S., Huang, W., Xu, H., Chen, T., Ke, Y., Qu, Z., Yan, N., 2020. Alkali-induced deactivation mechanism of $\text{V}_2\text{O}_5\text{-WO}_3/\text{TiO}_2$ catalyst during selective catalytic reduction of NO by NH_3 in aluminum hydrate calcining flue gas. *Appl. Catal. B-Environ.* 270, 118872.
- Li, G., Mao, D., Chao, M., Li, G., Yu, J., Guo, X., 2021a. Low-temperature $\text{NH}_3\text{-SCR}$ of NO over $\text{MnCeO}_2/\text{TiO}_2$ catalyst: enhanced activity and SO_2 tolerance by modifying TiO_2 with Al_2O_3 . *J. Rare. Earth.* 39, 805–816.

- Li, Y., Yang, S., Peng, H., Liu, W., Mi, Y., Wang, Z., Tang, C., Wu, D., An, T., 2021b. Insight into the activity and SO₂ tolerance of hierarchically ordered MnFe₁₋₈Co₈Ox ternary oxides for low-temperature selective catalytic reduction of NOx with NH₃. *J. Catal.* 395, 195–209.
- Lian, Z., Liu, L., Lin, C., Shan, W., He, H., 2022. Hydrothermal aging treatment activates V₂O₅/TiO₂ catalysts for NOx abatement. *Environ. Sci. Technol.* 56, 9744–9750.
- Liu, Y.-Z., Guo, R.-T., Duan, C.-P., Wu, G.-L., Miao, Y.-F., Gu, J.-W., Pan, W.-G., 2020a. A highly effective urchin-like MnCrOx catalyst for the selective catalytic reduction of NOx with NH₃. *Fuel* 271, 117667.
- Liu, Z., Chen, C., Zhao, J., Yang, L., Sun, K., Zeng, L., Pan, Y., Liu, Y., Liu, C., 2020b. Study on the NO₂ production pathways and the role of NO₂ in fast selective catalytic reduction DeNOx at low-temperature over MnOx/TiO₂ catalyst. *Fuel* 271, 117667.
- Liu, B., Liu, J., Xin, L., Zhang, T., Xu, Y., Jiang, F., Liu, X., 2021a. Unraveling reactivity descriptors and structure sensitivity in low-temperature NH₃-SCR reaction over CeTiOx catalysts: a combined computational and experimental study. *ACS Catal.* 11, 7613–7636.
- Liu, J., Cheng, H., Zheng, H., Zhang, L., Liu, B., Song, W., Liu, J., Zhu, W., Li, H., Zhao, Z., 2021b. Insight into the potassium poisoning effect for selective catalytic reduction of NOx with NH₃ over Fe β . *ACS Catal.* 11, 14727–14739.
- Liu, J., Ren, X., Zhang, Z., Sun, N., Tan, H., Cai, J., 2021c. Study on the mechanism of selective catalytic reduction of NOx by NH₃ over Mn-doped CoCr₂O₄. *J. Phys. Chem. C* 125, 14228–14238.
- Liu, J., Wu, X., Hou, B., Du, Y., Liu, L., Yang, B., 2021d. NiMn₂O₄ sphere catalyst for the selective catalytic reduction of NO by NH₃: insight into the enhanced activity via solvothermal method. *J. Environ. Chem. Eng.* 9, 105152.
- Lyu, Z., Niu, S., Lu, C., Zhao, G., Gong, Z., Zhu, Y., 2020. A density functional theory study on the selective catalytic reduction of NO by NH₃ reactivity of α -Fe₂O₃ (001) catalyst doped by mn, tiCr and Ni. *Fuel* 267, 117147.
- Nam, K.B., Lee, S.H., Hong, S.C., 2021. The role of copper in the enhanced performance of W/Ti catalysts for low-temperature selective catalytic reduction. *Appl. Sur. Sci.* 544, 148643.
- Pan, H., Gao, E.-H., Fang, T.-T., Mei, Y., He, Y., Shi, Y., 2021a. In situ treatment by high-temperature water vapor as a novel health-care approach for commercial SCR catalyst. *Appl. Sur. Sci.* 541, 148408.
- Pan, Y., Jin, Q., Lu, B., Ding, Y., Xu, X., Shen, Y., Zeng, Y., 2021b. New insights into MnCe(Ba)O/TiO₂ composite oxide catalyst: barium additive accelerated ammonia conversion. *J. Rare. Earth.* 39, 532–540.
- Peng, Y., Li, J., Chen, L., Chen, J., Han, J., Zhang, H., Han, W., 2012a. Alkali metal poisoning of a CeO₂-WO₃ catalyst used in the selective catalytic reduction of NOx with NH₃: an experimental and theoretical study. *Environ. Sci. Technol.* 46, 2864–2869.
- Peng, Y., Li, J., Shi, W., Xu, J., Hao, J., 2012b. Design strategies for development of SCR catalyst: improvement of alkali poisoning resistance and novel regeneration method. *Environ. Sci. Technol.* 46, 12623–12629.
- Qin, G., Zheng, J., Li, Y., Yang, Y., Liu, X., Han, X., Huang, Z., 2022. Tailor the crystal planes of MIL-101(Fe) derivatives to enhance the activity of SCR reaction at medium and low temperature. *J. Colloid Interface Sci.* 615, 432–444.
- Ren, D., Gui, K., Gu, S., 2021. Quantum chemistry study of SCR-NH₃ nitric oxide reduction on ce-doped γ -Fe₂O₃ catalyst surface. *Mol. Catal.* 502, 111373.
- Shen, Y., Deng, J., Impeng, S., Li, S., Yan, T., Zhang, J., Shi, L., Zhang, D., 2020. Boosting toluene combustion by engineering co-o strength in cobalt oxide catalysts. *Environ. Sci. Technol.* 54, 10342–10350.
- Shi, Y., Yi, H., Gao, F., Zhao, S., Xie, Z., Tang, X., 2021. Evolution mechanism of transition metal in NH₃-SCR reaction over Mn-based bimetallic oxide catalysts: structure-activity relationships. *J. Hazard. Mater.* 413, 125361.
- Tan, W., Wang, J., Li, L., Liu, A., Song, G., Guo, K., Luo, Y., Liu, F., Gao, F., Dong, L., 2020. Gas phase sulfation of ceria-zirconia solid solutions for generating highly efficient and SO₂ resistant NH₃-SCR catalysts for NO removal. *J. Hazard. Mater.* 388, 121729.
- Wang, S.-X., Guo, R.-T., Pan, W.-G., Chen, Q.-L., Sun, P., Li, M.-Y., Liu, S.-M., 2017. The deactivation of Ce/TiO₂ catalyst for NH₃-SCR reaction by alkali metals: TPD and DRIFT studies. *Catal. Commun.* 89, 143–147.
- Wang, Z., Lan, J., Haneda, M., Liu, Z., 2021. Selective catalytic reduction of NOx with NH₃ over a novel Co-Ce-Ti catalyst. *Catal. Today* 376, 222–228.
- Wei, Y., Fan, H., Wang, R., 2018. Transition metals (Co, zr, Ti) modified iron-samarium oxide as efficient catalysts for selective catalytic reduction of NOx at low-temperature. *Appl. Sur. Sci.* 459, 63–73.
- Wei, L., Wang, Z., Liu, Y., Guo, G., Dai, H., Cui, S., Deng, J., 2021. Support promotion effect on the SO₂ and K(+) co-poisoning resistance of MnO₂/TiO₂ for NH₃-SCR of NO. *J. Hazard. Mater.* 416, 126117.
- Wu, Z., Zeng, Y., Song, F., Zhang, S., Zhong, Q., 2019. Active sites assembly effect on CeO₂-WO₃-TiO₂ catalysts for selective catalytic reduction of NO with NH₃. *Mol. Catal.* 479, 110549.
- Wu, G.-L., Guo, R.-T., Liu, Y.-Z., Duan, C.-P., Miao, Y.-F., Gu, J.-W., Pan, W.-G., 2021. Promoting effect of Sb on the selective catalytic reduction of NO with NH₃ over CeVO₄ catalyst. *J. Energy Inst.* 95, 77–86.
- Xie, A., Tang, Y., Huang, X., Jin, X., Gu, P., Luo, S., Yao, C., Li, X., 2019. Three-dimensional nanoflower MnCrO/sepilolite catalyst with increased SO₂ resistance for NH₃-SCR at low temperature. *Chem. Eng. J.* 370, 897–905.
- Xue, H., Guo, X., Meng, T., Guo, Q., Mao, D., Wang, S., 2021. Cu-ZSM-5 catalyst impregnated with Mn-Co oxide for the selected catalytic reduction of NO: physicochemical property-catalytic activity relationship and in situ DRIFTS study for the reaction mechanism. *ACS Catal.* 11, 7702–7718.
- Yao, X., Chen, L., Cao, J., Chen, Y., Tian, M., Yang, F., Sun, J., Tang, C., Dong, L., 2019. Enhancing the deNO performance of MnO/CeO₂-ZrO₂ nanorod catalyst for low-temperature NH₃-SCR by TiO₂ modification. *Chem. Eng. J.* 369, 46–56.
- Yoon, W., Kim, Y., Jong Kim, G., Kim, J.-R., Lee, S., Han, H., Hyeon Park, G., Chae, H.-J., Bae Kim, W., 2022. Boosting low temperature De-NOx performance and SO₂ resistance over Ce-doped two dimensional Mn-Cr layered double oxide catalyst. *Chem. Eng. J.* 434, 134676.
- Youn, J.-R., Kim, M.-J., Lee, S.-J., Ryu, I.-S., Yoon, H.C., Jeong, S.K., Lee, K., Jeon, S.G., 2021. The influence of CNTs addition on Mn-Ce/TiO₂ catalyst for low-temperature NH₃-SCR of NO. *Catal. Commun.* 152, 106282.
- Yu, Y., Tan, W., An, D., Tang, C., Zou, W., Ge, C., Tong, Q., Gao, F., Sun, J., Dong, L., 2021. Activity enhancement of WO₃ modified FeTiO catalysts for the selective catalytic reduction of NO by NH₃. *Catal. Today* 375, 614–622.
- Zeng, Y., Song, W., Wang, Y., Zhang, S., Wang, T., Zhong, Q., 2020. Novel Fe-doped CePO₄ catalyst for selective catalytic reduction of NO with NH₃: the role of Fe(3+) ions. *J. Hazard. Mater.* 383, 121212.
- Zhang, J., Liang, J., Peng, H., Mi, Y., Luo, P., Xu, H., He, M., Wu, P., 2021. Cost-effective fast-synthesis of chabazite zeolites for the reduction of NOx. *Appl. Catal. B-Environ.* 292, 120163.
- Zheng, W., Zhang, X., Zheng, Y., Yue, Y., 2022. "Oxynitride trap" over N/S co-doped graphene-supported catalysts promoting low temperature NH₃-SCR performance: insight into the structure and mechanisms. *J. Hazard. Mater.* 423, 127187.